Received: 3 July 2019 | Revised: 30 September 2019 | Accepted: 1 October 2019
DOI: 10.1002/er.4958

RESEARCH ARTICLE

WILEY INTERNATIONAL JOURNAL OF ENERGY RESEARCH

Designing performance enhanced nuclear battery based on the Cd-109 radioactive source

Zhiheng Xu | **Zhangang Jin** | **Xiaobin Tang** | **Yunpeng Liu** | **Xiao Guo** | **Cong Peng** | **Hongyu Wang**

Department of Nuclear Science and Technology, Nanjing University of Aeronautics and Astronautics, Nanjing 211106, China

Correspondence
Xiaobin Tang, Department of Nuclear Science and Technology, Nanjing University of Aeronautics and Astronautics, Nanjing 211106, China.
Email: tangxiaobin@nuaa.edu.cn

Funding information
Fundamental Research Funds for the Central Universities, Grant/Award Number: NP2018462; Shanghai Aerospace Science and Technology Innovation Project, Grant/Award Number: SAST2016112; Jiangsu Planned Projects for Postdoctoral Research Funds, Grant/Award Number: 1601139B; National Natural Science Foundation of China, Grant/Award Number: 11675076

Summary
A dual-effect nuclear battery based on the radio-voltaic and radioluminescence effect was developed, which has the ability to convert nuclear energy into electrical energy with two different modes. Performance-enhanced nuclear batteries are mainly based on the addition of ZnS:Cu radio-luminescent layer to Cd-109 X-ray radioactive source and GaAs radio-voltaic layer. In order to explore the response relationship between the mode of energy conversion and the electrical performance of nuclear battery, the physical model was established to research the deposition energy distribution by using Monte Carlo method. The addition of the radio-luminescent material increases the effective energy deposition of the X-rays and the optimized thickness of ZnS:Cu in such a dual-effect nuclear battery should be set to 560 μm. The current–voltage characteristic curves of the batteries before and after performance optimization were utilized to investigate the electrical properties. Through a comprehensive comparison of Cd-109 nuclear batteries with or without radio-luminescent layer, the simulated results are consistent with experimental results. The results indicate that the electrical performance of dual-effect nuclear battery is significantly higher than that of single radio-voltaic nuclear battery. Moreover, the energy conversion efficiency increases from 0.079% (single radio-voltaic nuclear battery) to 0.119% (dual-effect nuclear battery). The improved performance of the dual-effect nuclear battery provides potential applications for space-based autonomous remote sensors and continuous low-power generation technologies.

KEYWORDS
dual-effect nuclear battery, energy conversion, Monte Carlo simulation, radio-luminescent, radio-voltaic

1 | INTRODUCTION

Nuclear batteries, also known as isotope batteries, use energy-carrying particles (such as alpha particles, beta particles, and gamma rays) that are emitted by radioactive isotope decay and convert their energy into electrical energy. The nuclear battery has the characteristics of light weight, small volume, long life, high power density, and no external replenishment energy.[1-3] With the development of the human aerospace industry, such batteries are urgently needed in deep space exploration, landing aircraft, and scientific discovery experiments in the space field. Space nuclear battery technology has also been listed by NASA as one of the top ten technological innovations for future space development. At present, nuclear batteries that have been applied in the field of aerospace mainly adopt the way of static energy conversion, and the radioisotope thermoelectric generator (RTG) is the main representative.[4-7] Pu-238 radioactive source is currently the most ideal isotope heat source for the RTG, but its production and preparation process is extremely difficult, the annual output is not high, and the price is expensive. At present, only Russia has a complete production line with a very limited production capacity. U.S. is also rebuilding its Pu-238 production line because of a shortage of existing Pu-238 stock.[8] Many researchers are also actively looking for alternative methods and trying other new energy conversion mechanisms.

In recent years, radio-voltaic nuclear battery and radio-luminescent nuclear battery are mainly developed for independent energy supply of space microelectronic components.[8-11] Both types of batteries are based on the kinetic energy of the radiation particles for energy conversion, which are the typical representative of the current research direction of micro-sized nuclear batteries. However, their electrical performance levels remain low and the output power often at the order of nW–μW.[12-16] The fundamental reason lies in the selection of radioactive sources and the way of energy conversion. In order to reduce the radiation damage of semiconductor materials and strive for a longer service life, these types of nuclear batteries try not to use high energy α and β radioisotopes as the excitation sources.[8,17-21] At the same time, for the α source and low energy β source with strong self-absorption effect of radiation particles, they severely limit the final output power and energy conversion efficiency of the nuclear battery to some extent.[22-24] Compared with α and β particle sources, the penetration power of X-ray or γ-ray is more stronger, and the corresponding self-absorption effect is very weak.[25,26] In the past, the infrequent use of X/γ sources in battery preparation is mainly due to radiation protection considerations. However, when it is in an outer space environment, the X/γ radioactive sources can be effectively used as energy sources for the nuclear batteries with suitable structure.[27,28]

In this study, a dual-effect nuclear battery based on radio-voltaic and radio-luminescent energy conversion mechanism was constructed and experimentally prepared with Cd-109 radioactive source, and optimized GaAs radio-voltaic layer and ZnS:Cu radio-luminescent layer. The new dual-effect nuclear battery takes advantages of radio-voltaic effect and radio-luminescent effect. The new nuclear battery uses a combination of these two effects, and its energy conversion efficiency is up to 50.63%, significantly higher than if it had just one. The complementary nuclear batteries can also achieve better performance by selecting X/γ radioactive sources with higher energy and setting up dual-effect mechanism with multi-layer structure.

2 | APPROACH

The X-ray energy spectrum of the Cd-109 radioactive source is depicted in Figure 1A, which was obtained by the HPGe detector (ORTEC GL0110P). The X-ray average energy of Cd-109 source is 23.79 keV. The Monte Carlo program MCNP5 was used to calculate the piercing power of 23.79 keV X-rays in Pb, as shown in Figure 1B. When the thickness of Pb reaches 50 μm, the X-ray energy can be shielded to a very low level. This also indicates that even considering the problem of radiation shielding, the dual-effect nuclear battery with Cd-109 source is conducive to miniaturization design. The X-ray energy spectrum was tested using the radiation detector system (CZT probe, Shanxi DETEK; Multichannel pulse amplitude analyzer, ORTEC 946; Preamplifier, ORTEC 572A).

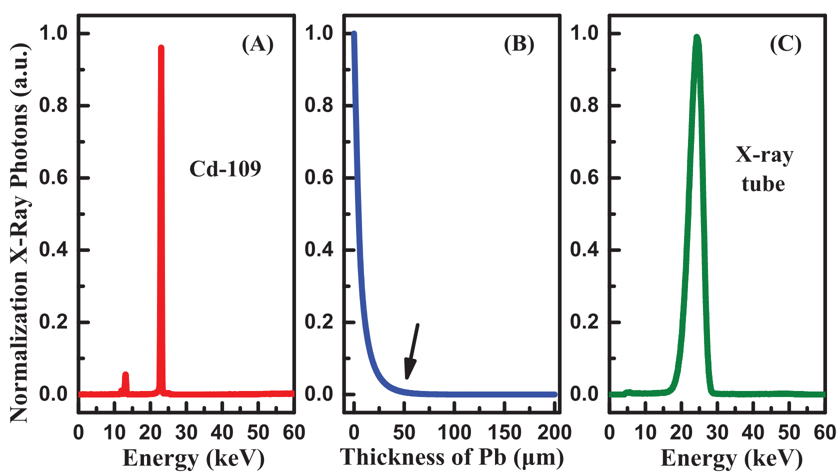

FIGURE 1 A, X-ray energy spectrum of Cd-109 radioactive source. B, the piercing power of 23.79 keV X-ray in Pb. C, X-ray energy spectrum emitted from 30 kV X-ray tube [Colour figure can be viewed at wileyonlinelibrary.com]

Figure 1C reflects that the peak energy from the X-ray tube is 23.76 keV, which is approximate to the particle average energy released by the Cd-109 source. The corresponding tube voltage and tube current were set to 30 kV and 900 μA, respectively. In order to better explore the laws and facilitate experimental operations, the X-ray tube (Shanghai KeyWay Electron Company Ltd. KYW900A) was used to instead of Cd-109 radioactive source to test the output performance of nuclear batteries.

The intensity (I_X) of the X-ray tube consumption of electric energy to generate X-rays can be expressed as:

$$I_X = K_i \times V^2 \times i \times Z \quad (1)$$

where K_i is a constant (1.1~1.3 × 10^{-6}), V is the X-ray tube voltage (kV), i is the X-ray tube current (mA), and Z is the atomic number of the X-ray tube target (tungsten, $Z = 74$). The power of the emitted X-rays under the experimental conditions can be calculated to be 0.054 W. If the average energy of a single X-ray particle is assumed to be 23.76 keV, the number of X-ray particles generated per second by the X-ray tube is approximately 1.42 × 10^{13}. MCNP5 was used to simulate and calculate the number of the emitted X-ray particles, and the parameters set by the model are consistent with the experiment. The distance between the beryllium window and the tungsten target is set to 3.1 mm, the thickness of the window is 200 μm, the diameter of the target is 1 mm, and the radiation angle is 20°. The calculation result is 3.46 × 10^{11}, which is approximately equivalent to 9.4 Ci Cd-109 source.

A size of 10 mm × 10 mm × 0.375 mm GaAs PN junction was designed as the radio-voltaic layer. The structural parameters, such as the window layer, the emitter region, and the base region, are shown in Figure 2A. The substrate occupies most of the thickness of the radio-voltaic layer, about 360 μm. MCNP5 was used to simulate the X-ray particle deposition behavior in GaAs, with each layer set to a thickness of 10 μm. Figure 2B displays the attenuation curve of X-rays in GaAs, where most of the X-ray energy of Cd-109 source can be deposited in the radio-voltaic layer.

3 | RESULTS AND DISCUSSION

3.1 | Single radio-voltaic nuclear battery performance analysis

A single radio-voltaic nuclear battery with three GaAs radio-voltaic layers was modelled. The actual power is generated from the window layer, the emitter, and the base regions of the radio-voltaic layer. Set the radio-voltaic layer closest to the excitation source to the first layer, and so on. According to the MCNP5 calculation results given in Figure 3A, the radiant energy deposition of the first layer is 2.03 × 10^3 times that of the second layer and 5.73 × 10^5 times that of the third layer.

Assuming that the X-ray energy deposition in the window layer, the emitter region, and the base region of the radio-voltaic layer are completely used to generate electron–hole pairs, the short-circuit current generated by the radio-voltaic effect ($I_{\text{sc-R}}$) can be expressed as:

$$I_{\text{sc-R}} = \frac{q \times E_v}{E_{\text{ehp}}} = \frac{q \times E_v}{2.8 \times E_g + 0.5} \quad (2)$$

where q is the elementary charge, E_v is the effective energy deposited in the radio-voltaic layer, E_{ehp} is the

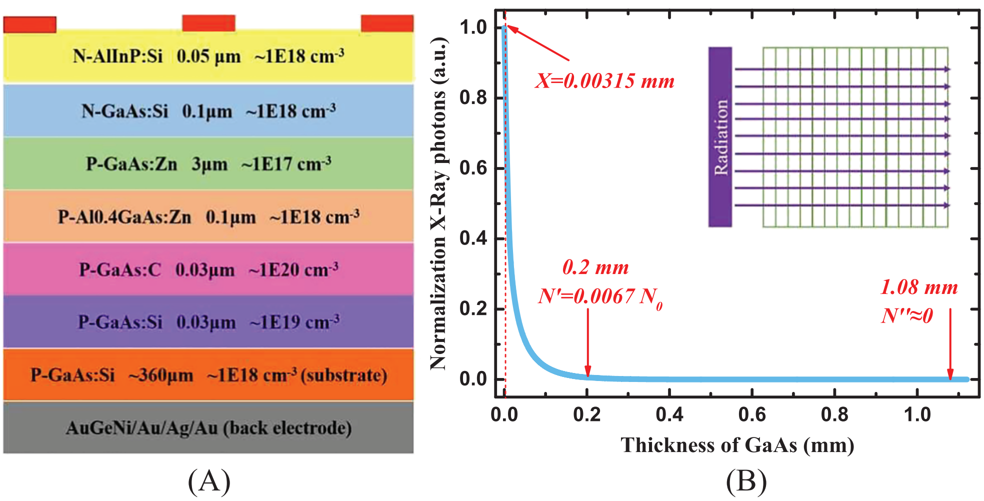

FIGURE 2 A, Structure diagram of GaAs radio-voltaic layer. B, Attenuation behavior of Cd-109 X-ray in GaAs, the illustration is a schematic diagram of the model [Colour figure can be viewed at wileyonlinelibrary.com]

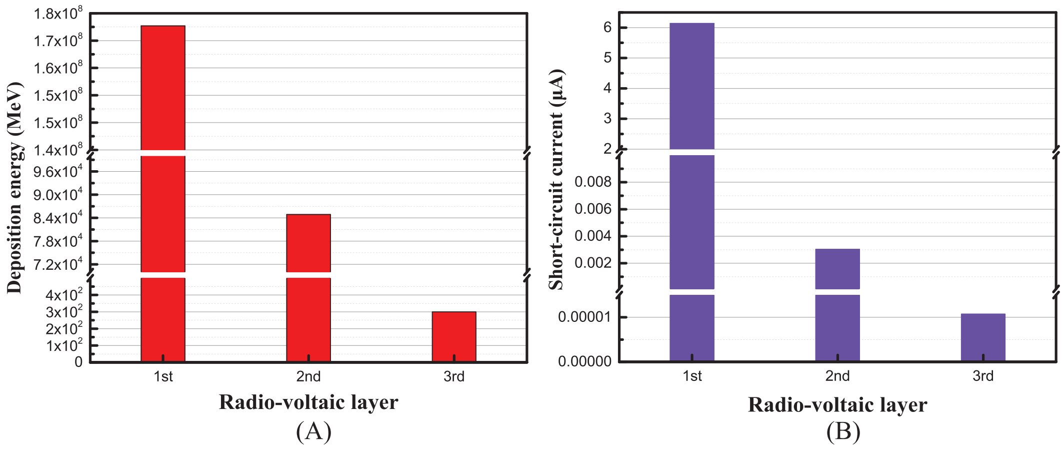

FIGURE 3 A, Effective deposition energy in each radio-voltaic layer. B, Current generated in each radio-voltaic layer [Colour figure can be viewed at wileyonlinelibrary.com]

electron–hole pair ionization energy, E_g is the band-gap of semiconductor material, which is 1.42 eV for GaAs. Figure 3B shows the calculation results of the $I_{sc\text{-}R}$ for each radio-voltaic layer. The value of $I_{sc\text{-}R}$ of the first radio-voltaic layer is 2026 times than that of the second layer, which is 572594 times than that of the third layer. For such a single radio-voltaic nuclear battery, the first layer is a major contributor to overall performance output. Therefore, minimizing the substrate thickness and increasing the utilization of X-ray energy can improve the electrical performance of the battery.

The thinnest radio-voltaic layer used in nuclear batteries is diamond, which is prepared by ion-implantation assisted lift-off method and has a thickness of 17.5 μm.[29] The GaAs radio-voltaic layer structure remains unchanged, and the overall thickness can be controlled to 20 μm by thinning the thickness of the substrate. The previous three-layer radio-voltaic layer continued to be extended to ten layers, and Figure 4A shows the energy deposition of each layer. Furthermore, the open-circuit voltage (V_{oc}) of the battery can be calculated by Equation 3,

$$V_{oc} = \frac{k_B \times T_a}{q} \times \ln\left(\frac{I_{sc}}{I_0} + 1\right) \tag{3}$$

where k_B is the Boltzmann constant, T_a is the room temperature (300 K), I_{sc} is the short-circuit current, and I_0 is the saturation current. I_{sc} can be calculated by Equation (2). For GaAs radio-voltaic layer, I_0 has been measured by a dual-channel system source-meter instrument (Keithley, Model 2636A) and the value is 1.34 nA. Figure 4B shows the current and voltage for each of the ten GaAs radio-voltaic layers. The electrical performance parameters of each layer are different but they are all of the same magnitude. Therefore, each layer can be reasonably connected in series or in parallel to achieve greater output performance and meet the actual demand of the power-consuming devices.

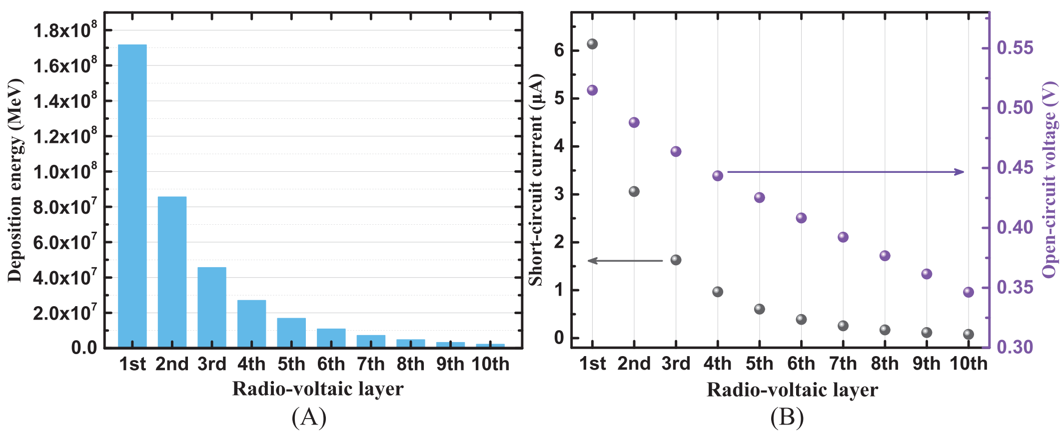

FIGURE 4 A, Effective deposition energy in each radio-voltaic layer. B, Electrical performance output parameters of each radio-voltaic layer [Colour figure can be viewed at wileyonlinelibrary.com]

3.2 | Proposed dual-effect nuclear battery design

The nuclear battery performance is highly influenced by the excitation source and energy conversion efficiency. Increasing the number of the radio-voltaic layer in a unit size can increase the utilization of radiant energy, thereby increasing the efficiency of the battery. In view of the operational difficulties of the substrate thinning technology, this work proposes a new plan. A dual-effect nuclear battery is prepared by combining two different energy conversion mechanisms. The configuration and working principle of the dual-effect nuclear battery is depicted in Figure 5. X-rays released from the decay of Cd-109 source directly on the GaAs radio-voltaic layer. A large number of electron–hole pairs by ionization and excitation in the semiconductor material, which are separated by the action of a built-in electric field and form the radio-voltaic current. On the other hand, X-rays excite ZnS:Cu radio-luminescent layer to produce fluorescent photons, which are then absorbed by GaAs layer to produce electron–hole pairs through the photovoltaic effect. These electron–hole pairs are also collected to form the radio-photovoltaic current. These two currents constitute the final output current of the dual-effect nuclear battery. To increase the conversion efficiency and output power, a 30 μm aluminum film was used as a luminescent reflective layer, which was coated on the irradiated surface of the ZnS:Cu layer.[30-33]

The X-ray radio-luminescent spectrum of the ZnS:Cu was measured with a Cary Eclipse fluorescence spectrophotometer (Agilent Technologies G9800a, Malaysia). The quantum efficiency curve of the GaAs was performed by quantum efficiency test system (Bentham, PVE300). During the test at normal temperature and pressure, these samples were optically and magnetically shielded to prevent interference. The coupling matching effect between ZnS:Cu radio-luminescent layer and GaAs radio-voltaic layer is excellent, and the radio-luminescent spectrum is almost in the photovoltaic response range, as shown in Figure 6. The spectrum curve shows a Gaussian distribution with a peak wavelength of about 528 nm, and the corresponding quantum efficiency is quite high.

The X-rays bombard the radio-luminescent material to cause it to excite, and then the radiation deposition energy is converted into luminescence of a specific wavelength. The corresponding radio-luminescence intensity (I_l) can be expressed as:

$$I_l = E_l \times \frac{h\nu}{2.67E_g + 0.87} \tag{4}$$

where E_l is the energy deposition of the radio-luminescent material, $h\nu$ is the energy of radio-luminescent photons at the peak wavelength, and E_g is the band-gap of the radio-luminescent material.[34,35] For ZnS:Cu used in this work, $h\nu$ is equal to 2.3 eV and E_g is equal to 3.8 eV. This also implies that the more effective radiation energy is deposited in the radio-luminescent material, the more fluorescent photons are generated.

There is also a self-absorption effect in the transport process of fluorescent photons from the place where they are generated to the emitting surface. Fluorescent photons undergo loss behaviors such as absorption and scattering during transport before reaching the surface of the radio-voltaic layer. Therefore, the effective radio-luminescence intensity ($I_{l\text{-eff}}$) actually reaching the surface of the radio-voltaic layer can be calculated using the following equations:

$$I_{l-\mathrm{eff}} = I_l \times e^{-(K+S)l} \tag{5}$$

$$K + S = \frac{\ln^{I_l}/_{I_{l-\mathrm{eff}}}}{l} = \frac{\ln^{1}/_{T}}{l} \tag{6}$$

where K is the absorption coefficient, S is the scattering coefficient, l is the thickness of the radio-luminescent

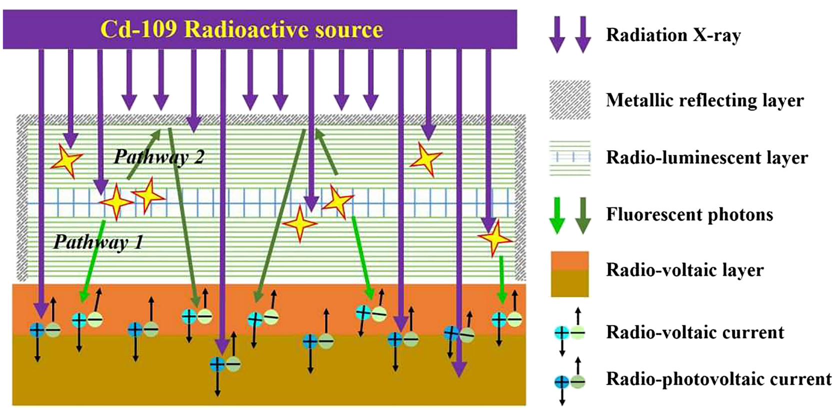

FIGURE 5 The schematic of Cd-109 dual-effect nuclear battery [Colour figure can be viewed at wileyonlinelibrary.com]

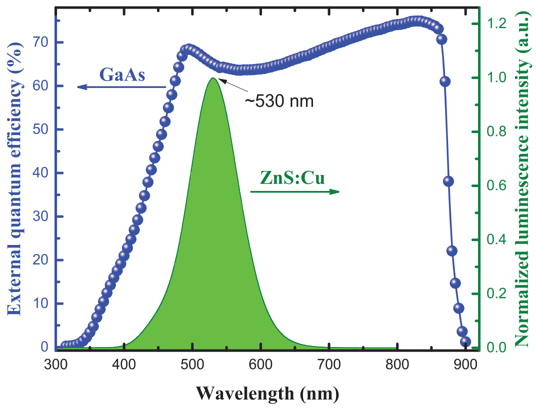

FIGURE 6 Emission spectrum of ZnS:Cu radio-luminescent layer and external quantum efficiency curve of GaAs radio-voltaic layer [Colour figure can be viewed at wileyonlinelibrary.com]

layer, T is the transmittance.[36] Two ideal conditions are set here: 1) the radio-luminescent photons generated in the ZnS:Cu layer are uniform and isotropic, and 2) the reflectivity of the aluminum film to luminescen photons is 100%. The optical transmittance of different thickness ZnS:Cu layers was measured with a Shimadzu 3600 UV–VIS–NIR spectrophotometer (Figure 7A). The thinner the thickness, the higher the transmittance, which is more conducive to the transmission of fluorescent photons. Conversely, the thicker the radio-luminescent layer, the more radiation energy that can be deposited and the ability to produce more photons. Figure 7B illustrates the linear fitting of transmittance with the thickness of ZnS:Cu layer. According to Equation (6), the sum of the absorption coefficient and the scattering coefficient is 0.01088 μm^{-1}. So based on the competitive relationship, there is a trade-off between the various effects. The thickness of the ZnS:Cu layer needs to be designed to a suitable value to optimize battery performance.

3.3 | Theoretical analysis of dual-effect nuclear battery

ZnS:Cu radio-luminescent layers with various thickness were prepared and analyzed taking into account the dual energy conversion mechanism and the characteristics of the selected materials. The thickness of the GaAs radio-voltaic layer and the aluminum reflector were maintained at 375 μm and 30 μm, respectively. The single layer thickness of the ZnS:Cu layer is 70 μm, and the number of layers can be added according to the actual test needs. The nuclear battery without ZnS:Cu layer is defined as S0, with single-layer ZnS:Cu layer defined as S1, and with double-layer defined as S2, and similarly, with nine layers defined as S9.

MCNP5 was performed to simulate the X-rays deposition on the different thickness ZnS:Cu layers. The area of the ZnS:Cu layer is 10 mm × 10 mm, and the thickness thereof is divided into a plurality of layers, and each layer is set to 5 μm. According to Equations (4) and (5), the total radio-luminescence intensity ($I_{\text{l-tot}}$) can be determined by the following formulas:

$$I_{\text{l-tot}} = 0.5\sum_{n=1}^{N} I_n \left(e^{-5(K+S)n} + e^{-5(K+S)(2N-n)}\right) \tag{7}$$

$$I_{\text{n}} = E_{\text{n}} \times \frac{h\nu}{2.67E_{\text{g}} + 0.87} \tag{8}$$

where n is the count number of the ZnS:Cu layer, N is the total number of the ZnS:Cu layers divided, and E_{n} is the radiation deposition energy of the nth layer. Figure 8A and B show the deposition energy and the total radio-luminescence intensity of the ZnS:Cu layer. As the number of the ZnS:Cu layer increases, the fraction of

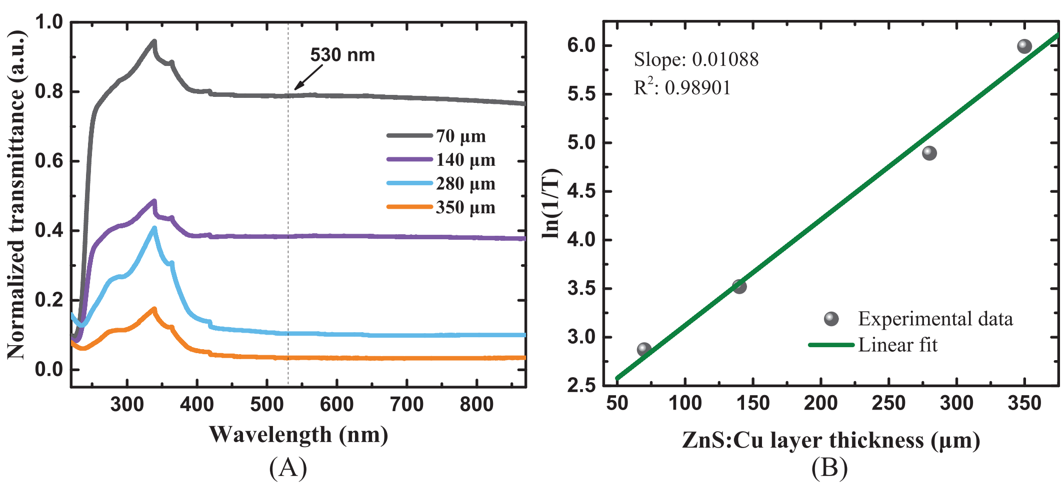

FIGURE 7 A, Transmission spectra of ZnS:Cu radio-luminescent layer with different thicknesses. B, A linear fit between transmittance and radio-luminescent layer thickness [Colour figure can be viewed at wileyonlinelibrary.com]

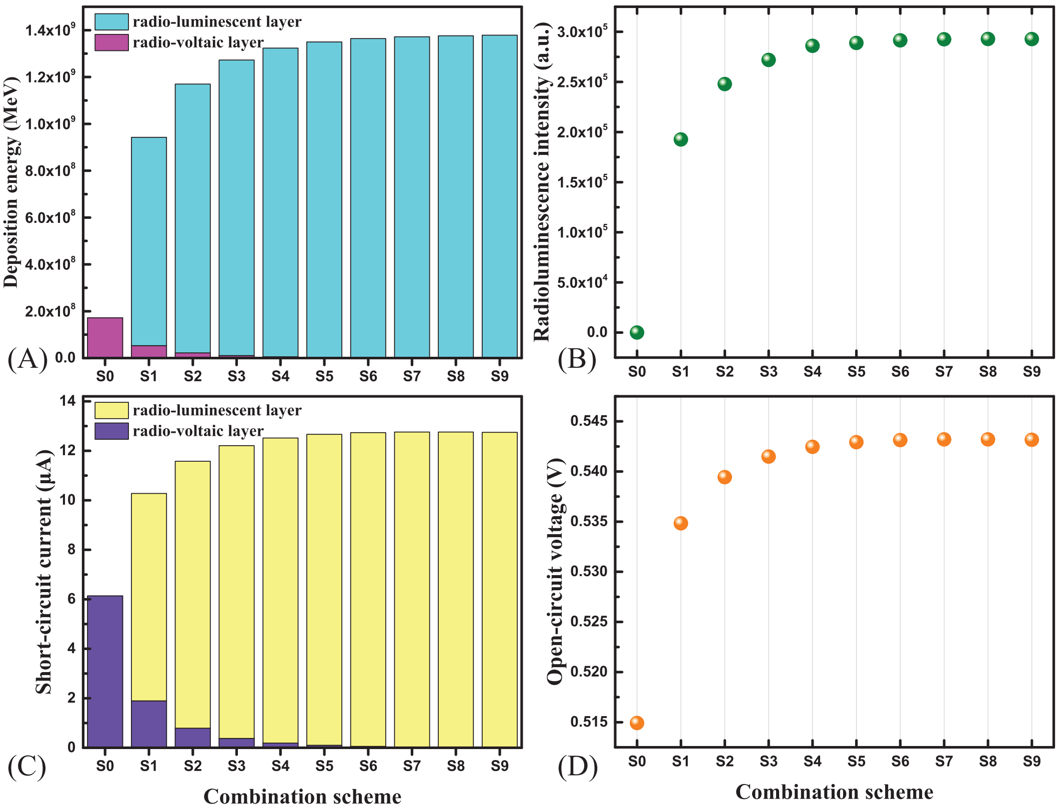

FIGURE 8 Performance parameters for different combination schemes: A, Deposition energy. B, Radio-luminescence intensity. C, $I_{\text{sc-R}}$ and $I_{\text{sc-P}}$. D, V_{oc} of nuclear batteries with different combination schemes. S0 − S9 represent different radio-luminescent layer thickness [Colour figure can be viewed at wileyonlinelibrary.com]

radiant energy deposited gradually increases until it becomes saturated, as well as the total radio-luminescence intensity. In such a structure, when the thickness of the ZnS:Cu layer is increased to about 560 μm, the intensity starts to reach a saturation value.

Assuming the fluorescent photons are completely captured by the radio-voltaic layer, and the photocurrent ($I_{\text{sc-P}}$) generated based on the photovoltaic effect can be expressed as,

$$I_{\text{sc-P}} = q\int_{E_g}^{\infty} QE(E) \times b_s(E, T_a)dE \tag{9}$$

where $QE(E)$ is the quantum response efficiency of the radio-voltaic layer, $b_s(E, T_a)$ is the photon flux density and can be obtained from the radio-luminescence spectrum. The radio-voltaic current $I_{\text{sc-R}}$ in Equation (2) and the radio-photovoltaic current $I_{\text{sc-P}}$ in Equation (9) constitute the final output total current of the dual-effect nuclear battery. Figure 8C indicates the response relationship between the output current of the battery and the number of the radio-luminescent layers. The trend of current variation with the thickness of the ZnS:Cu layer is similar to that of energy deposition. The increase in the ZnS:Cu layer significantly increases the output current of the nuclear battery compared to the GaAs radio-voltaic layer alone. For the single radio-voltaic nuclear battery (S0 scheme), the short-circuit current is 6.14 μA. When the thickness of the ZnS:Cu layer is 560 μm (S8 scheme), the current can reach about 12.76 μA, a relative increase of 2.08 times. Adding the ZnS:Cu layer as an energy conversion medium can increase the output open-circuit voltage of the nuclear battery (Figure 8D).

3.4 | Dual-effect nuclear battery performance test

Based on the above theoretical design and simulation analysis results, single radio-voltaic nuclear battery and dual-effect nuclear battery were prepared. The material type and parameters used in the battery are consistent with the simulation. The dual-effect nuclear battery uses a design of a 560 μm ZnS:Cu layer and a 30 μm aluminum reflective film, as shown in Figure 9A. The electrical properties of these two types of nuclear batteries were tested under the excitation of X-ray radiation. Figure 9B illustrates the corresponding current–voltage ($I - V$) and power-voltage ($P - V$) characteristic curves of different combinatorial nuclear batteries.

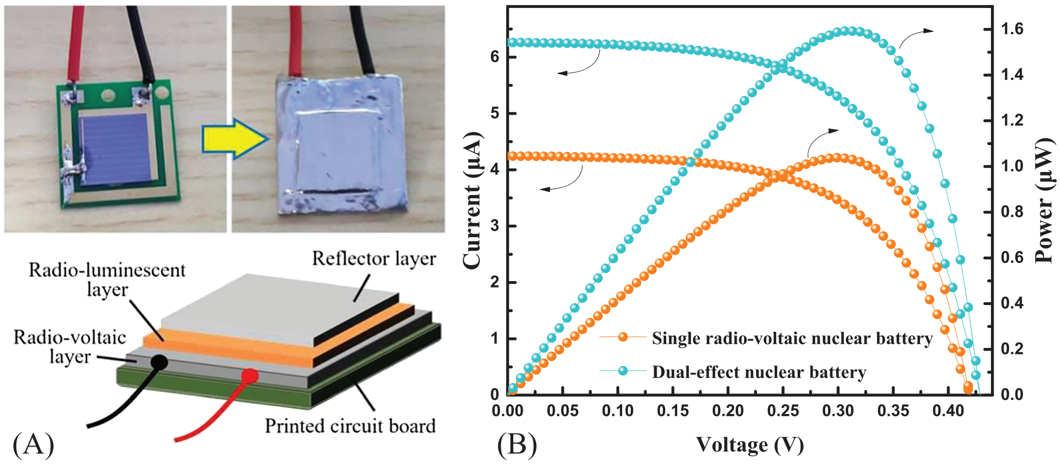

FIGURE 9 A, Nuclear battery samples and structure schematic. B, $I-V$ and $P-V$ characteristic curves of nuclear battery before and after performance enhancement [Colour figure can be viewed at wileyonlinelibrary.com]

The values of I_{sc} and V_{oc} extracted from these curves are compared with the theoretical simulation calculations as shown in Table 1. The total energy conversion efficiency (η_{total}) of the nuclear battery can be expressed as:

$$\eta_{total} = \frac{P_{max}}{E_X} = \frac{V_{mp} \times I_{mp}}{A \times E_{X-av}} \tag{10}$$

where P_{max} is the maximum value of the product of the current and voltage in the $I-V$ characteristic curves, V_{mp} and I_{mp} are the corresponding current and voltage at the maximum power value, A is the number of X-rays emitted per second, and $E_{X\text{-}av}$ is the average energy of X-rays. The current and power of the dual-effect nuclear battery are significantly improved compared with the single radio-voltaic nuclear battery. P_{max} and η_{total} increased by 52.88% and 50.63%, respectively. The improvement in battery performance verifies that the radio-luminescent layer and the reflective layer help to enhance the absorption of radiant energy and the collection of luminescent photons. The change trend of theoretical values also coincided with experimental values. This means that Monte Carlo simulation analysis can predict battery output performance to some extent. Some electrical performance parameters have certain differences, especially the current, which is mainly due to the following reasons: 1) the energy deposited in the GaAs layer cannot be completely used to generate electron–hole pairs, and some are also lost in the form of heat; 2) the electron–hole pairs cannot be fully collected and will also be captured and recombined; 3) the reflection effect of the aluminum film is not 100%, and the photons are also absorbed. These aspects are the cause of energy loss and the direction of efforts to improve battery performance.

TABLE 1 Electrical performance parameters of nuclear batteries.

Electrical properties		Single radio-voltaic nuclear battery	Dual-effect nuclear battery
I_{sc} (μA)	Theoretical value	6.14	12.76
V_{oc} (V)	Theoretical value	0.51	0.54
I_{sc} (μA)	Experimental value	4.25	6.26
V_{oc} (V)	Experimental value	0.42	0.43
P_{max} (μW)	Experimental value	1.04	1.59
η_{total} (%)	Experimental value	0.079	0.119

4 | CONCLUSIONS

In summary, a small nuclear power source based on Cd-109 X-ray source is developed using Monte Carlo simulation optimization and experimental test verification. Energy optimal consumption and efficient luminescence transport is considered by improving the overall output performance of the nuclear power source. The dual-effect nuclear battery based on the radio-voltaic and radioluminescence effects was introduced and successfully implemented. A variety of different strategies are employed to optimize energy utilization and improve battery conversion efficiency, such as spectral response matching, radio-luminescent layer thickness optimization, and reflective layer design. Under the premise that the excitation source remains unchanged, the use of the ZnS:Cu radio-luminescent layer and the aluminum reflective film increases the maximum output power of the nuclear battery from 1.04 μW to 1.59 μW.

In this work, X-ray source is effectively used in nuclear battery preparation, breaking the inherent thinking limit of using pure beta source. Meanwhile, the radioluminescent materials can be used to cut down the sensitivity of the semiconductor components to radiation. The proposed approach based on the carrier transport process is constructed working at nuclear power source optimization by balancing the energy conversion methods and regulating the output performance. Overall, the newly proposed dual-effect nuclear battery can be more conducive to energy management strategies than single radiovoltaic nuclear battery, which can increase output power and prolong the service life.

ACKNOWLEDGEMENTS

This work was financially supported by the National Natural Science Foundation of China (Grant no. 11675076), the Jiangsu Planned Projects for Postdoctoral Research Funds (Grant no. 1601139B), the Shanghai Aerospace Science and Technology Innovation Project (Grant no. SAST2016112), and the Fundamental Research Funds for the Central Universities (Grant no. NP2018462).

ORCID

Zhiheng Xu https://orcid.org/0000-0002-9229-8558
Xiaobin Tang http://orcid.org/0000-0003-3308-0468

REFERENCES

1. Bower KE, Barbanel YA, Shreter YG, Bohnert GW. *Polymers, phosphors, and voltaics for radioisotope microbatteries*. Boca Raton (USA): CRC Press; 2002:31-60.
2. Olsen LC, Cabauy P, Elkind BJ. Betavoltaic power sources. *Phys Today*. 2012;65(12):35-38.
3. Xu ZH, Zhang ZR, Chen W, et al. $CsPbBr_3$ quantum dot films with high luminescence efficiency and irradiation stability for radioluminescent nuclear battery application. *ACS Appl Mater Interfaces*. 2019;11(15):14191-14199.
4. Rowe DM. Applications of nuclear-powered thermoelectric generators in space. *Appl Energy*. 1991;40(4):241-271.
5. O'Brien RC, Ambrosi RM, Bannister NP, Howe SD, Atkinson HV. Safe radioisotope thermoelectric generators and heat sources for space applications. *J Nucl Mater*. 2008;377(3):506-521.
6. Yuan ZC, Tang XB, Xu ZH, et al. Screen-printed radial structure micro radioisotope thermoelectric generator. *Appl Energy*. 2018;225:746-754.
7. Liu K, Tang XB, Liu YP, et al. Preparation and optimization of miniaturized radioisotope thermoelectric generator based on concentric filament architecture. *J Power Sources*. 2018;407:14-22.
8. Prelas M, Boraas M, De La Torre Aguilar F, Seelig J, Tchakoua Tchouaso M, Wisniewski D. *Nuclear batteries and radioisotopes*. Switzerland: Springer International Publishing; 2016:103-155.
9. Chen CC, Chang YY, Zhang JW. A novel betavoltaic microbattery based on SWNTs thin film-silicon heterojunction. In: *2012 IEEE 25th International Conference on Micro Electro Mechanical Systems (MEMS)*. France, Paris;2012:1197–1200.
10. Russo J, Litz M, Ray W II, Rosen GM, Bigio DI, Fazio R. Development of tritiated nitroxide for nuclear battery. *Appl Radiat Isot*. 2017;125:66-73.
11. Xu ZH, Liu YP, Zhang ZR, et al. Enhanced radioluminescent nuclear battery by optimizing structural design of the phosphor layer. *Int J Energ Res*. 2018;42(4):1729-1737.
12. Kim T, Lee N, Jung HK, Kim HJ. Enhancement of energy performance in betavoltaic cells by optimizing self-absorption of beta particles. *Int J Energy Res*. 2016;40(4):522-528.
13. Zhang Q, Chen R, San H, Liu G, Wang K. Betavoltaic effect in titanium dioxide nanotube arrays under build-in potential difference. *J Power Sources*. 2015;282:529-533.
14. Thomas C, Portnoff S, Spencer MG. High efficiency 4H-SiC betavoltaic power sources using tritium radioisotopes. *Appl Phys Lett*. 2016;108(1):013505.
15. Artun O. A study of nuclear structure for ^{244}Cm, ^{241}Am, ^{238}Pu, ^{210}Po, ^{147}Pm, ^{137}Cs, ^{90}Sr and ^{63}Ni nuclei used in nuclear battery. *Mod Phys Lett A*. 2017;32(22):1750117.
16. Rahastama S, Waris A. Analytical study of ^{90}Sr betavoltaic nuclear battery performance based on p-n junction silicon. *J Phys Conf Ser*. 2016;739(1):012003.
17. Liu YP, Tang XB, Xu ZH, et al. Influences of planar source thickness on betavoltaics with different semiconductors. *J Radioanal Nucl Chem*. 2015;304(2):517-525.
18. Guo X, Liu YP, Xu ZH, et al. Multi-level radioisotope batteries based on ^{60}Co γ source and Radio-voltaic/Radio-photovoltaic dual effects. *Sensor Actuat A-Phys*. 2018;275:119-128.
19. Russo J, Litz M, Ray IIW, et al. Demonstration of a tritiated nitroxide nuclear battery. *Appl Radiat Isot*. 2019;144:93-103.
20. Prelas MA, Weaver CL, Watermann ML, Lukosi ED, Schott RJ, Wisniewski DA. A review of nuclear batteries. *Prog Nucl Energ*. 2014;75:117-148.
21. Prelas MA, Tchouaso MT. High efficiency Dual-Cycle Conversion System Using Kr-85. *Appl Radiat Isot*. 2018;139:70-80.
22. Zhang ZR, Tang XB, Liu YP, et al. GaAs radiovoltaic cell enhanced by Y_2SiO_5 crystal for the development of new gamma microbatteries. *Nucl Instrum Meth B*. 2017;398:35-41.
23. Landis GA, Bailey SG, Clark EB, et al. Non-solar photovoltaics for small space missions. In: *2012 38th IEEE Photovoltaic Specialists Conference (PVSC)*. USA, Austin;2012:002819–002824.
24. Alam TR, Spencer MG, Prelas MA, Pierson MA. Design and optimization of radioisotope sources for betavoltaic batteries. *Int J Energ Res*. 2018;42(7):2564-2573.
25. Lee H, Yim MS. Examination of scintillator-photovoltaic cell-based spent fuel radiation energy conversion for electricity generation. *Prog Nucl Energy*. 2017;94:46-54.
26. Jin ZG, Tang XB, Guo X. Design and performance study of four-layer radio-voltaic and dual-effect nuclear batteries based on γ-ray. *Nucl Instrum Meth B*. 2018;428:47-55.
27. Butera S, Whitaker MDC, Lioliou G, Barnett AM. AlGaAs ^{55}Fe X-ray radioisotope microbattery. *Sci Rep*. 2016;6(1):38409.
28. Butera S, Lioliou G, Krysa AB, Barnett AM. $Al_{0.52}In_{0.48}P$ ^{55}Fe X-ray-photovoltaic battery. *J Phys D Appl Phys*. 2016;49(35):355601.

29. Bormashov VS, Troschiev SY, Tarelkin SA, et al. High power density nuclear battery prototype based on diamond Schottky diodes. *Diamond Relat Mater*. 2018;84:41-47.

30. Sychov M, Kavetsky A, Yakubova G, et al. Alpha indirect conversion radioisotope power source. *Appl Radiat Isot*. 2008;66(2):173-177.

31. Xu ZH, Tang XB, Hong L, et al. Development of a beta radioluminescence nuclear battery. *Nucl Sci Tech*. 2014;25(4):040603.

32. Zhang ZR, Tang XB, Liu YP, et al. Application of liquid scintillators as energy conversion materials in nuclear batteries. *Sensor Actuat A-Phys*. 2019;290:162-171.

33. Zhang ZR, Liu YP, Tang XB, et al. GaAs Low-energy X-ray radioluminescence nuclear battery. *Nucl Instrum Meth B*. 2018;415:9-16.

34. William MY, Shigeo S, Hajime Y. *Phosphor handbook (Second edition)*. Boca Raton: CRC Press; 2018:140-143.

35. Hong L, Tang XB, Xu ZH, Liu YP, Chen D. Parameter optimization and experiment verification for a beta radioluminescence nuclear battery. *J Radioanal Nucl Ch*. 2014;302(1):701-707.

36. Smith WJ. *Modern optical engineering*. Tata McGraw-Hill Education (USA): SPIE Press; 2008:205-210.

How to cite this article: Xu Z, Jin Z, Tang X, et al. Designing performance enhanced nuclear battery based on the Cd-109 radioactive source. *Int J Energy Res*. 2020;44:508–517. https://doi.org/10.1002/er.4958